

PACS numbers: 52.38.Mf; 78.67.–n; 81.07.–b; 81.16.Nd; 82.35.Np
DOI: 10.1070/QE2010v040n10ABEH014442

Laser generation of nanostructures on the surface and in the bulk of solids

N.M. Bityurin

Abstract. **This paper considers nanostructuring of solid surfaces by nano-optical techniques, primarily by laser particle nanolithography. Threshold processes are examined that can be used for laser structuring of solid surfaces, with particular attention to laser swelling of materials. Fundamental spatial resolution issues in three-dimensional (3D) laser nanostructuring are analysed with application to laser nanopolymerisation and 3D optical information recording. The formation of nanostructures in the bulk of solids due to their structural instability under irradiation is exemplified by photoinduced formation of nanocomposites.**

Keywords: *laser nanostructuring, nanolithography, ablation, swelling, nanopolymerisation, nanocomposites.*

1. Introduction

Nanostructuring of materials has a significant effect on their physical and chemical properties, which underlies many advanced nanotechnologies. Owing to recent advances in laser systems, laser radiation is one of the most effective tools for modifying materials. At the same time, the fabrication of nanostructures using the most readily available visible and near-UV lasers presents the problem of overcoming the diffraction limit in focusing the laser beam. To produce nanostructures by laser pulses, the laser radiation field should be highly localised, in particular using near-field optics. This can be achieved by a variety of techniques [1], including those that employ field enhancement beneath an atomic force microscope tip [2], near-field optical microscope probes, various near-field masks and interference lithography [3]. A promising area of research is so-called laser particle nanolithography [3–6]: fabrication of submicron- and nanometre-scale structures via laser radiation field localisation using transparent micro- and nanospheres placed on the surface of the material (Fig. 1).

This method requires no expensive equipment. An ordered array of spheres results from either self-organisation [3] or optical trapping, in particular using Bessel beam optical traps [7].

It is commonly thought that an array of dielectric spheres focuses incident laser light as though the spheres act independently of each other. It was however shown [8] that femtosecond laser pulses incident on a close-packed layer of microspheres having their backside coated with gold produced hexagonal rather than circular holes (Fig. 2). This finding attests to significant laser radiation rescattering effects in the system. As seen in Fig. 2, the apertures possess sixfold symmetry. Such interference effects may be very important in laser-assisted particle nanolithography and may result in unexpected phenomena, which should be investigated and employed [9]. To date, this issue has been addressed in only two reports [8, 10] and the effects in question are still not thoroughly understood.

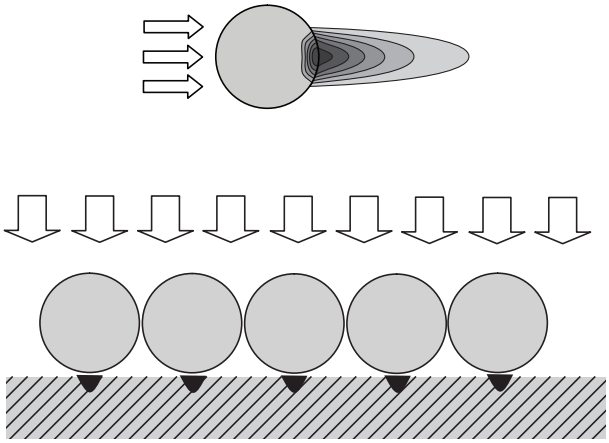

Figure 1. Schematic illustrating the principle of nanosphere lithography.

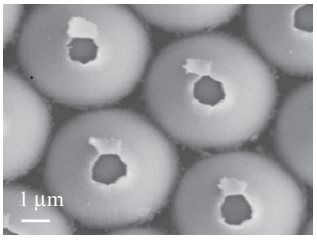

Figure 2. Scanning electron microscope image of apertures produced by exposing a monolayer of gold-coated microspheres (radius r_{sp} = 3.4 μm, index of refraction n = 1.77) to femtosecond laser pulses (λ = 800 nm). Figure adapted from Pikulin et al. [8].

Along with optical field localisation, a strong nonlinear response of a material to laser radiation can be used for nanostructuring. Surface modification and nanostructuring can be achieved using not only nonlinear absorption but also nonlinear effects with feedback, e.g. photothermochemical insta-

N.M. Bityurin Institute of Applied Physics, Russian Academy of Sciences, ul. Ulyanova 46, 603950 Nizhnii Novgorod, Russia; e-mail: bit@appl.sci-nnov.ru

Received 19 August 2010
Kvantovaya Elektronika **40** (11) 955–965 (2010)
Translated by O.M. Tsarev

bility [11, 12], and threshold effects, such as laser ablation, melting, swelling and polymerisation.

It would be expected from Fig. 3 that, near the modification threshold, the modified zone could be made as small as desired by reducing the energy absorbed during laser exposure, even when the laser beam has a comparatively large diameter. Note at the same time that the size of the resulting nanofeature is also influenced by the nonlocal response of the material to the laser exposure.

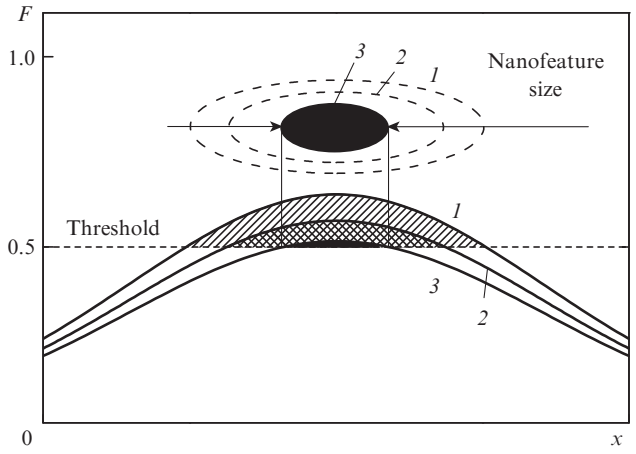

Figure 3. Schematic illustrating the laser modification of materials with a threshold response: (*1–3*) absorbed energy (*F*) distributions. Figure adapted from Pikulin and Bityurin [13].

Nanostructured materials can also be produced by laser exposure that, even when homogeneous, gives rise to instabilities, leading to the formation of nanoclusters or nanoinhomogeneities in an initially homogeneous material. The development of inhomogeneities typically has a significant effect on the optical properties of such materials, which may be of considerable practical interest. In this context, the ability to produce materials capable of such nanostructuring under laser irradiation is critical.

Section 2 considers laser-induced surface modification processes, such as ablation and swelling. Attention is paid primarily to laser swelling – the least studied, and nevertheless very promising, effect, which is used for the surface nanostructuring primarily of polymers and glasses. Section 3 is concerned with three-dimensional (3D) structuring by highly focused laser beams and considers laser polymerisation, which is currently one of the most viable approaches to producing 3D nanostructures. Section 4 addresses issues pertaining to the formation of nano-objects in initially homogeneous solids exposed to laser radiation, which is not necessarily focused: irradiation gives rise to instabilities, which are responsible for the formation of nanoinhomogeneities. Major attention is paid to the photoinduced formation of metal-organic composites.

2. Laser-induced surface modification: swelling

Laser ablation, a technique for polymer surface processing via layer-by-layer material removal by laser pulses, has been extensively studied in the past 25 years. The main trends in the development of this technique were reviewed elsewhere [12]. In particular, a model was constructed for the laser ablation of strongly absorbing polymers by nano- and femtosecond laser pulses [14]. Note, however, that there is no appropriate model for the ablation of weakly absorbing polymers and that the specifics of the ablation of such polymers with femtosecond laser pulses have not been fully investigated. Such data would be very helpful for accurately assessing the potential of laser ablation for nanostructuring. There are the first experimental data on the nanostructuring of polymer surfaces by laser ablation with femtosecond pulses using dielectric microspheres, and further research is obviously needed.

Convex surface structures can be produced through laser swelling with no material removal. Laser exposure of polymers and polymer-like materials below the ablation threshold produces a bump (hump) (Fig. 4).

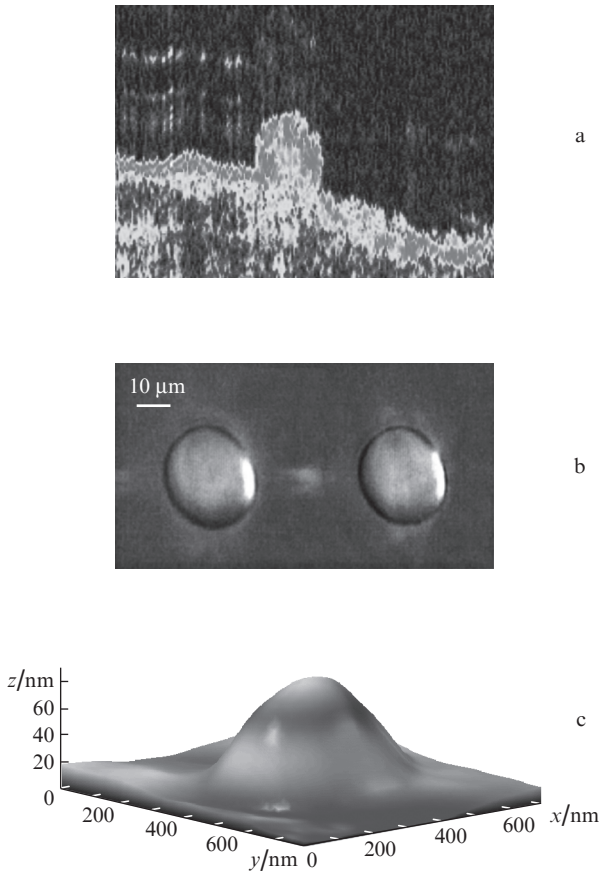

Figure 4. Formation of humps (swelling) on the surface of polymers and polymer-like materials: (a) swelling of biological tissue (optical coherence tomography image) [15]; (b) swelling of coloured PMMA exposed to focused frequency-doubled Nd:YAG laser radiation (micrograph) [16]; (c) nanoswelling caused by laser radiation incident on a polymer surface containing microspheres (atomic force microscope image) [17].

This effect may be due to both expansion of the irradiated material and substance redistribution over the surface through hydrodynamic effects. There is still no commonly accepted terminology in this area of research, but the former process is usually referred to as laser swelling, whereas the formation of bumps on an initially smooth surface exposed to laser radiation is often referred to as bumping. In producing nanofeatures, swelling is preferable because the response of the material to irradiation is then more local. Swelling is also of interest

because it leads to the formation of regions with an increased free volume. The kinetics of chemical reactions in polymer matrices are sensitive to the free volume. Therefore, laser swelling can be used to produce surface nanostructures with enhanced reactivity. Given that chemical reactions in 'nanoreactors' have a number of special features, it is reasonable to anticipate that studies of laser-induced surface nanostructuring through swelling will give interesting, unexpected results. Porous convex structures can be selectively doped with luminescent dyes.

Laser swelling was probably first detected and studied experimentally by Fukumura et al. [18], who investigated the effect of XeCl excimer laser radiation on dye-doped poly(methyl methacrylate) (PMMA). The swelling of the polymer was used later to generate an array of optical microlenses on the surface of PMMA doped with photochemically decomposable substances [19]. Phillips and Sauerbrey [20] used swelling to produce a periodic surface profile by two coherent laser beams.

Nanoswelling is essentially unexplored. There is experimental evidence that this effect can be used for nanostructuring [7, 17], but there have not been any detailed studies on the feasibility of producing nanostructures using swelling or the application of such nanostructures.

Theoretical modelling of swelling is crucial for a fundamental understanding of this effect. Himmelbauer et al. [21, 22] reported experimental and theoretical studies of swelling in polyimide exposed to UV laser radiation. The swelling was attributed to amorphisation, resulting in the melting of the polycrystals present in the material, followed by rapid cooling, so that the polycrystals remained amorphous. Since the density of amorphous materials is lower, amorphisation is accompanied by the formation of convex structures on polymer surfaces.

This and similar models, however, fail to account for transient swelling. Several studies were concerned with transient swelling caused by UV irradiation of undoped PMMA and other polymeric materials with various chromophore additions [23–25]. The point is that the surface swelling immediately after a laser pulse may substantially exceed that a considerable time after the exposure. Such transient swelling cannot be accounted for solely by thermal expansion. A number of reports attributed the swelling of polymeric materials to the laser-induced generation of volatile species in the polymer [19, 26–28].

Crucial for understanding this process is that laser exposure may lead to the formation of gas molecules in the polymer. At a sufficiently high temperature, this would generate a pressure high enough to deform the polymer matrix and, hence, to cause swelling.

Small molecules may be formed through chemical reactions leading to the decomposition of the polymer or additives. The main argument for such interpretation of swelling is not the unsteady-state phase, which is usually not investigated, but the presence of bubbles beneath the surface when the swelling threshold is substantially exceeded, which is thought to be evidence of gas generation. Gas generation in irradiated materials is, of course, of special importance in the case of soft biological tissues, which consist to a significant degree of water. Gas generation is here of a physical, rather than chemical, nature because it is associated with water evaporation by laser heating. Kamensky et al. [15] experimentally studied laser swelling dynamics in a cataractous lens exposed to free-running Er:KGSS laser radiation (λ = 1.54 μm) (Fig. 4a). As shown by Malyshev and Bityurin [29], the key features of biological tissue swelling can be modelled in terms of tissue water evaporation, which generates pressure and distorts the protein basis of the tissue, with allowance for water molecule transfer in the gas phase in the distorted substance in the presence of a liquid phase.

In the case of synthetic polymers, however, swelling cannot be attributed only to small molecules. In particular, Masubuchi et al. [24] examined swelling of undoped PMMA films on quartz and argued that generation of small particles could be neglected, even though the irradiation wavelength was 248 nm, i.e. short enough to cause generation of small particles.

Malyshev et al. [16] experimentally studied the swelling of dye-doped PMMA exposed to frequency-doubled Nd:YAG laser radiation (Figs 4b, 4c). They observed significant swelling even though photochemical and thermochemical reactions were precluded. The swelling threshold was evaluated as a function of absorption coefficient, which was determined in their experiments by the dye concentration, and the residual hump height (due to swelling) was measured as a function of laser fluence. Their results showed that, at near-threshold laser pulse energy densities, the generation of surface bumps by laser irradiation was due to an increase in volume, whereas the substance redistribution effect prevailed when the pulse energy density exceeded the swelling threshold by about 30% (Fig. 5).

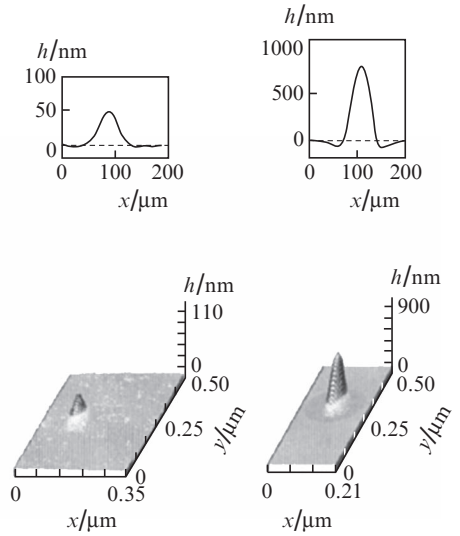

Figure 5. Surface profiles measured with a ZYGO microinterferometer after laser exposure of a polymer sample. The left profile corresponds to an increase in volume, i.e. to swelling (near-threshold pulse energy density). The right-hand profile corresponds to substance redistribution caused by laser exposure at a relatively high pulse energy density (the volume of the substance after the laser exposure is roughly the same as before). Figure adapted from Malyshev et al. [16].

A number of studies concerned with the generation of convex structures by short laser pulses interpreted the mechanism underlying the formation of such structures in terms of mechanical relief and tensile stress generation in the irradiated sample just after the laser pulse [30–32].

Malyshev and Bityurin [30] proposed a model in which the formation of a bump on the surface of a polymeric material exposed to sufficiently short laser pulses was attributed to

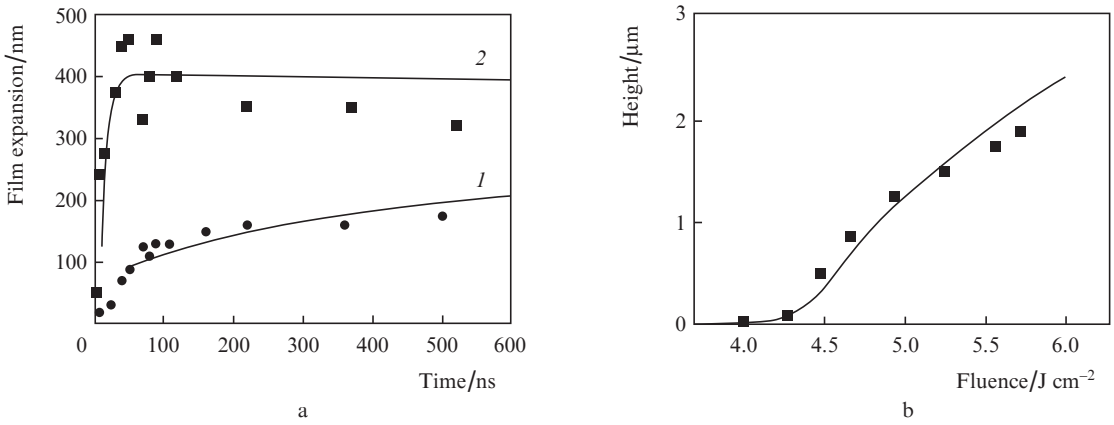

Figure 6. Comparison of calculation results for laser swelling in the relaxation model with experimental data. The points represent (a) swelling dynamics data [24] and (b) the residual swelling height as a function of laser fluence [16]. The solid lines show calculation results in (a) point and (b) distributed models. Curves (*1*) and (*2*) represent data for different laser pulse energies.

mechanical stress arising from optical energy absorption. The absorption of a short (nanosecond) laser pulse results in a thermoelastic stress wave, which propagates into the bulk of the material. The thermoelastic wave consists of two components: the pressure arising at the leading edge of the laser pulse (negative stress) gives way to pressure relief (positive tensile stress). In brittle materials at room temperature, the stress relief wave may cause failure and spallation of the material. At the same time, if a laser pulse heats the material to about its softening temperature, the positive stress (relief) in the wave gives rise to elastoplastic strain in the heated region. The net (peak) strain is then the sum of the thermal expansion, elastic and plastic strains.

After the relaxation of the elastic and thermal expansion strains, the irreversible plastic strain determines the height of the bump. The characteristic time for deformation of the material and the formation of a bump with the maximum height corresponds to the time needed for the thermoelastic relief wave to traverse the heated region.

Zhakhovskii et al. [31] and Lazare et al. [32] attributed swelling to the formation of micro- and nanocavities in the irradiated region during the stress relief described above. This effect is quite similar to cavitation in a 'tensile' liquid, can be described by the theory of first-order phase transitions and appears very interesting for nanostructuring of materials through laser-induced instability development. At the same time, surface nanoswelling near the swelling threshold seems to follow a different mechanism.

As early as 2001, Masubuchi et al. [24] assumed swelling to be associated with the transition of the polymer to a rubbery state, which has a significantly greater thermal expansion coefficient in comparison with the glassy state. They however did not take into account the salient feature of this state: its slow response to changes in external conditions. Therefore, one should take into account the relaxation nature of thermal expansion near the glass transition temperature of amorphous materials. Relaxation theory of the swelling of polymers, which accounts well for laser swelling dynamics in polymer films assessed with nanosecond precision [24], has been formulated very recently [33]. The relaxation model for laser swelling attributes it to the transition of the polymer to a rubbery state on laser heating and the reverse transition during subsequent cooling of the material. The model takes into account the relaxation nature of the transition and the temperature dependence of the relaxation time. It can be shown that experimental data on the swelling of dye-doped PMMA exposed to nanosecond frequency-doubled Nd:YAG laser pulses [16] and swelling dynamics in undoped PMMA exposed to 248-nm KrF excimer laser radiation [24] fit well with the relaxation model (Fig. 6).

Thus, near the ablation threshold the swelling seems to have a relaxation nature. Since plastic flow generally causes no increase in total volume, the experimental finding that swelling proper occurs near the bumping threshold, whereas at higher energy fluxes deformation is accompanied by no volume changes, may be interpreted as evidence of a transition from the relaxation model to a plasticity model in the stress relief step. Note that stress relief may produce cavities [31, 32], which have no time enough to collapse during rapid cooling of the irradiated region after the laser pulse because the viscosity of the material is a strong function of temperature.

3. 3D structuring and laser nanopolymerisation

In contrast to the laser effects above (ablation and swelling), two-photon laser polymerisation enables structuring not on the surface but in the bulk of a medium. Owing to the excellent optical and mechanical properties of such structures, this approach finds application in photonics, surface micromachining and 3D optical information storage. The most versatile technique for producing 3D nanostructures is sequential processing of a polymerisable medium using a well-focused laser beam. Femtosecond lasers offer the possibility to effectively use two-photon absorption for polymerisation initiation. Because there is nonlinear absorption and a single-shot gelation threshold, the process takes place only in a small region around the beam spot. The forming blob of polymer gel, commonly referred to as a voxel, may be less than 100 nm in size [34–36]. Translating the sample relative to the beam by a precision positioning system, one can create 3D patterns composed of individual voxels [37]. Photopolymerisation, a key step in this process, has been studied for more than six decades now, but only relatively recently have advances in laser technologies enabled micron- and submicron-scale polymerisation [38, 39]. Even though laser polymerisation has been the subject of intense experimental studies, very little work has been directed towards theoretical modelling of the process.

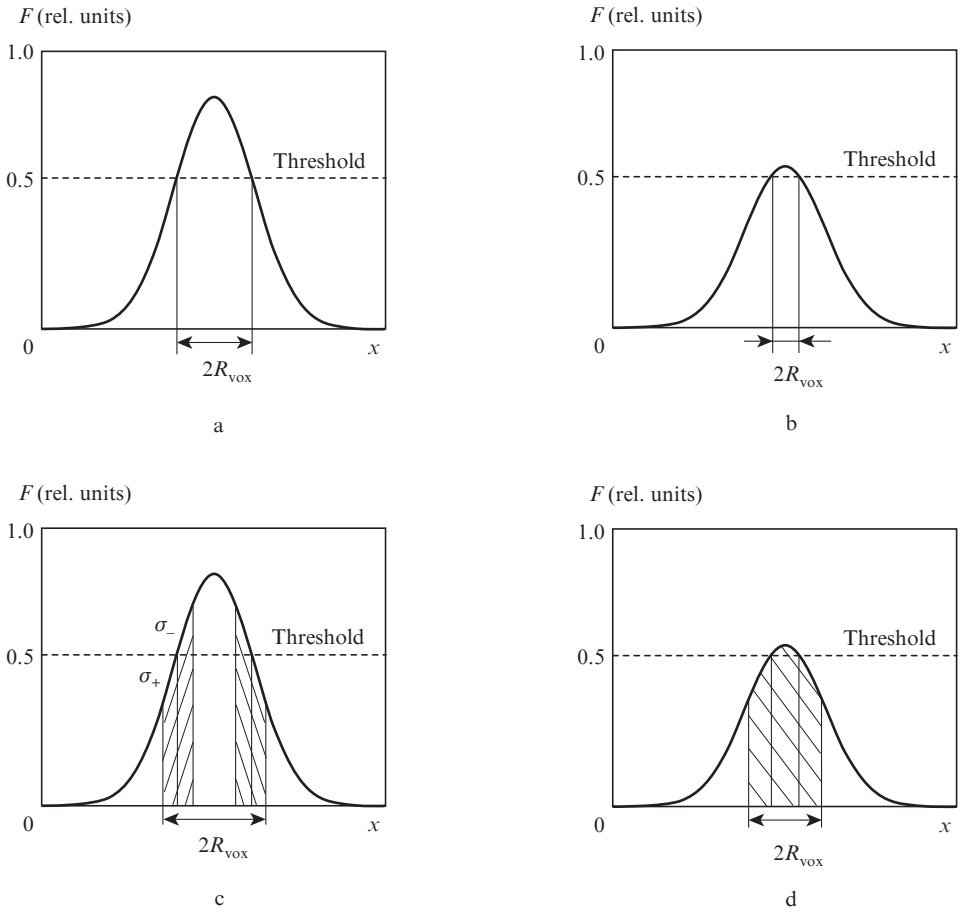

Figure 7. Schematic illustrating the fabrication of a small voxel by laser exposure using a threshold response of the material: (a, b) ideal case in which any small increase in intensity (or in appropriate integral characteristics of the exposure) above the threshold produces a voxel, which can thus be made as small as desired; (c, d) percolation transition as a threshold process in which σ_+ and σ_- fluctuation zones form at the voxel boundary. When the threshold is exceeded only slightly, the resultant voxel has a purely fluctuational nature (d) (R_{vox} is the voxel radius).

In laser nanopolymerisation, the threshold for the response of a substance to laser exposure is determined by a percolation transition associated with the formation of gel: a 3D network of macromolecules. In the case of homogeneous polymerisation, the percolation transition has a threshold in terms of the monomer conversion to polymer. Recent work [13] has shown however that the minimum size of nanofeatures produced by laser nanopolymerisation is limited by random inhomogeneities in the network of polymer molecules (Fig. 7). When the threshold is exceeded only slightly, the resultant voxel has a purely fluctuational nature. The properties of such voxels were studied by Pikulin and Bityurin [13]. It has been shown that different implementations of fluctuation voxels are dissimilar. The centroid and size of voxels fluctuate from implementation to implementation, and the number of voxels may differ from unity. In other words, irradiation results are irreproducible under such conditions. To produce reproducible voxels, these should have a nonfluctuating core, as shown in Fig. 7c. Pikulin and Bityurin [13] derived a generalised analytical formula for various spatial distributions of the monomer conversion to polymer. This formula can be used to estimate the minimum radius of a reliably produced voxel with negligible fluctuations. To this end, the results of the existing gradient percolation theory (percolation at a given spatial distribution of the percolation parameter) were generalised to a wider range of spatial distributions compared to those considered in the literature. The formula was verified using Monte Carlo simulation.

In addition to the creation of a voxel of minimum size, an important issue is the spatial resolution of two neighbouring voxels, which requires to take into account the nonlocal response of the material to laser exposure. This problem was addressed previously [40] for the fabrication of nanostructures via two-photon polymerisation by focused femtosecond laser pulses.

A theoretical approach was proposed which made it possible to take into account the diffusion of growing polymer chains during laser-induced radical nanopolymerisation [40]. Taking into consideration the decrease in the diffusion coefficient of particles with increasing particle size made it possible to construct a successive approximation procedure which took into account the diffusion of growing macromolecules only for short chains. For a typical case where the time needed for laser-assisted polymerisation initiation in a given region is much shorter than the polymerisation time, it is shown that the polymerisation process can be broken down into a fast stage, where diffusion is important, and a slow stage, where long chains grow and their diffusion can be neglected. An equation has been derived which allows one to find the distribution of the concentration of growing nondiffusing chains when the spatial distribution of the laser radiation that initiates the polymerisation process is known.

This approach allows one to estimate the minimum separation between two individual nanofeatures produced by laser polymerisation (Fig. 8). The critical length scale in particular systems capable of polymerising was estimated at 30–70 nm.

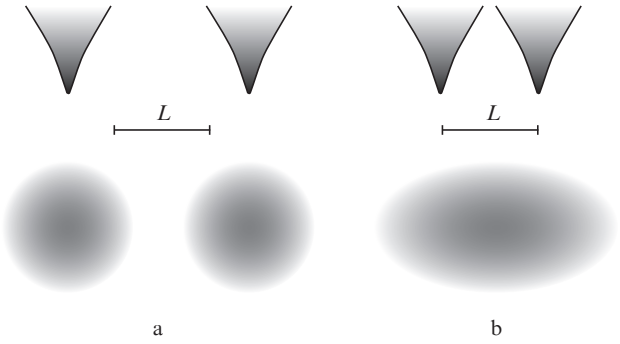

Figure 8. Schematic illustrating the problem of resolving two features: (a) two features are spatially resolved; (b) one feature is written instead of two.

Consider now how to maximise the recording density of a 3D array of voxels using focused laser beams. We are dealing with parasitic, cross-talk recording, where recording of other voxels produces noise for a given voxel. This problem was solved for a 3D photochemical bitwise laser-assisted information recording, but it is also important, e.g., for the laser polymerisation considered above. The point is that the irradiation time of an array of voxels for initiating polymerisation is considerably shorter than the polymerisation time, so spurious irradiation may be significant in this case as well.

3D bitwise information recording is usually performed by consecutive (parallel) focusing of a laser beam (laser beams) onto the position (positions) of a bit (bits). The problem is however that, when 1 is written in a given position, cross-talk recording in neighbouring positions is inevitable. The associated limitations were discussed in Ref. [41] for the case where recording was performed using single- and two-photon absorption of laser radiation.

Bityurin et al. [41] introduced a quantity characterising the spurious recording level: the ratio of the number of photons absorbed at a given point when unity is written into all other points to the number of photons that would be absorbed at a given point when unity is written into it (Fig. 9). We introduce

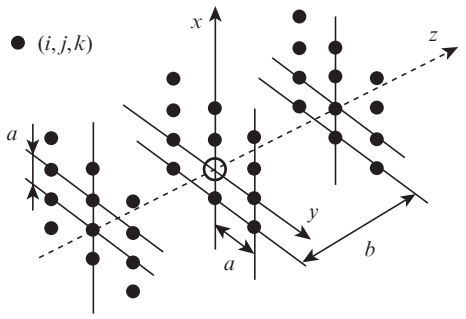

Figure 9. Schematic illustrating cross-talk recording in 3D bitwise laser-assisted information recording. When unity is written into all points except $(0,0,0)$, the ratio of the number of photons absorbed at this point to that needed to write 1 should not exceed η.

the concept of permissible cross-talk recording level, η. The laser beams are taken to be Gaussian.

Analysis of single-photon recording indicates that, to maintain the cross-talk recording level below the permissible level, an increase in the number of layers should be accompanied by an increase in the distance between bits in the layers. The main argument for 3D optical information recording is the increase in recording density per unit surface area owing to the third dimension. As shown previously [41], increasing the number of layers to above unity does not increase the surface recording density in the case of single-photon photochemical recording because of the limitations associated with cross-talk recording. Therefore, 3D single-photon information recording is ineffective.

At the same time, analysis of two-photon information recording indicates that, for a given permissible spurious exposure, there is an optimal configuration of recording points which maximises the volume recording density. In particular, at a numerical aperture of the objective NA = 1, refractive index of the medium $n = 1.5$, wavelength $\lambda = 800$ nm and permissible spurious recording level $\eta = 0.1$, the volume recording density ρ may reach 3×10^{13} bit cm^{-3}. This means that a disk 12 cm in diameter and 0.5 mm in thickness may contain about 20 Tbytes of information. At $\eta = 0.1$, the separation between the layers will be 0.75 μm. Thus, the disk will have 670 layers. The permissible spurious exposure level is determined by the reading procedure. At NA = 1 and $\eta = 0.7$, such a disk may contain 65 Tbytes of information.

In addition to the spatial resolution of laser structuring, an important issue is the sensitivity of materials to laser exposure. Considerable attention has been paid in the literature to the ability to improve the sensitivity of materials to femtosecond laser pulses by varying the characteristics of pulses, in particular, the pulse shape. Recent developments in the field were reviewed by Englert et al. [42]. In addition, they studied the influence of two pulses with a variable time delay between them or used phase modulation to obtain a sequence of pulse trains with a relatively strong first pulse, followed by a sequence of weaker pulses, and compared the influence of such trains to that of an inverse sequence of pulses. In the former case, the surface modification threshold for wide-gap dielectrics was lower than that in the latter case. The reason for this is that the first, strong pulse promotes electrons to the conduction band through multiphoton ionisation, whereas the weaker 'tail' acts on the conduction electrons, leading to impact ionisation. In the latter case, the weak leading edge has an insignificant effect on the substance. We believe however that preionisation effects can be realised most effectively by employing a higher frequency pulse as a forerunner. This issue was addressed in detail by Bityurin and Kuznetsov [43], who proposed using a bichromatic pulse comprising the fundamental frequency and the second harmonic. The second harmonic is intended to ensure efficient multiphoton ionisation, and the fundamental harmonic is more effective from the viewpoint of impact ionisation.

According to their results [43], partial upconversion to the second harmonic in 3D modification of a substance by highly focused femtosecond laser pulses involving ionisation may considerably reduce both the single- and multiple-shot modification thresholds (Fig. 10).

The electron energy distribution in the conduction band can be analysed using the Fokker–Planck equation in a double flux approximation [43]. The results show that, in the case of a rectangular laser pulse and electron multiplication through

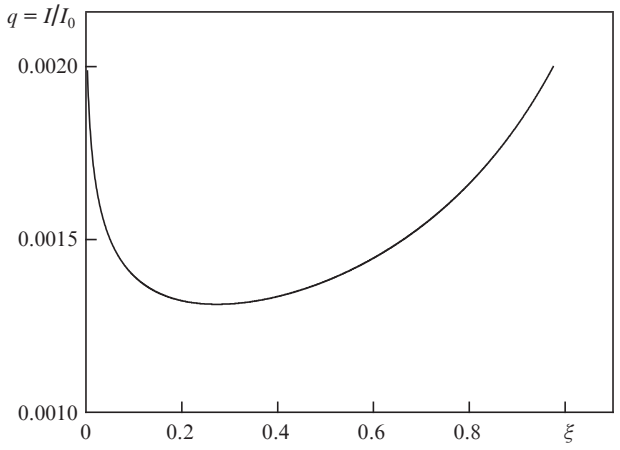

Figure 10. Typical plot of the breakdown intensity against the fraction of the energy converted to the second harmonic; I is the incident intensity and I_0 is the 'atomic' intensity used for normalisation.

impact ionisation, one should take into account the time delay between the onset of the laser pulse and impact ionisation onset. It is shown that, in the case of single-shot modification, the use of the second harmonic may markedly improve the multiphoton ionisation efficiency, whereas the fundamental harmonic is more effective for impact ionisation. There is an optimal second-harmonic energy conversion efficiency.

Multiple-shot modification was considered for substances with a high concentration of electron traps [44]. Such substances include e.g. titania gels and related organic–inorganic hybrid materials [45–49]. In such materials, the concentration of filled traps increases from pulse to pulse. Each pulse ionises filled traps rather easily (e.g. through single-photon absorption), and the concentration of conduction band electrons rises owing to impact ionisation. In the case of multiple-shot exposure, partial conversion to the second harmonic leads to efficient ionisation of deeper traps, markedly improving the process efficiency and considerably reducing the number of laser pulses needed for significant modification of the material.

It is of interest to note that exposure of materials containing traps to weakly focused high-power femtosecond laser pulses was observed to cause filling of the traps with electrons through two-photon absorption: one photon at the fundamental frequency and the other from the supercontinuum generated by the high-power laser radiation passing through the substance [50].

4. Nanostructuring of materials through irradiation-induced instability development and photoinduced formation of nanocomposites

Consider irradiation-induced instability development in initially homogeneous materials. Instability development leads to the formation of nanoclusters. Major attention is paid to the photoinduced formation of metallic nanoclusters, i.e. nanocomposites.

Nanocomposites containing semiconductor and metal nanoclusters embedded in a dielectric matrix have recently attracted a great deal of researchers' attention owing to their unique physical, chemical and optical properties [51–55]. Of particular interest is the synthesis of gold nanoparticles because of their high chemical stability, in particular to long-term oxidation [51].

The most widespread chemical method for the preparation of nanoparticles is the reduction of metal compounds in solution in the presence of various stabilisers. Typical reductants are hydrogen and its compounds. Moreover, because of the large specific surface area of nanoparticles, the fabrication of nanocomposites requires various stabilisers, among which the most widely used are surfactants and macromolecules.

Alexandrov et al. [56] and Smirnova et al. [57] proposed a novel approach to the fabrication of polymer-matrix nanocomposites. Its distinctive feature is that nanoparticles are not implanted into the polymer but produced directly in a polymer matrix by reducing dopants, e.g. chloroauric acid, $HAuCl_4$.

The key feature of this approach is that the polymer serves several functions, acting on the one hand as a matrix for nanoparticles and on the other as a stabiliser intended to prevent nanoparticle aggregation and ensure uniform nanoparticle distribution throughout the polymer and temporal stability of the nanocomposite.

The polymeric binder used was PMMA, which was selected for several reasons. In particular, PMMA-based films possess high optical transmission, being inferior only to silica glass, and can be used as optically transparent media with a near-zero absorption at wavelengths down to 290 nm [58]. Moreover, such polymer matrices have good physical and mechanical properties and a wide solubility range, which makes them attractive for producing films and bulk materials for optical applications.

Gold nanoparticles were prepared by combining UV exposure and heat treatment of a sample in the form of a $HAuCl_4$-doped polymer matrix. Films 20 to 200 μm in thickness were produced by coating and spin-coating with PMMA solutions. The atomic gold precursor in the film was $HAuCl_4$, which was added to a polymer solution. The formation of gold nanoparticles was initiated by UV irradiation of the $HAuCl_4$-containing PMMA films. As a UV source, we used a DRP-400 high/medium pressure mercury lamp or a XeCl excimer laser. After the initiation step, irradiation was ceased and the samples were thermostated. The experimental procedure is schematised in Fig. 11.

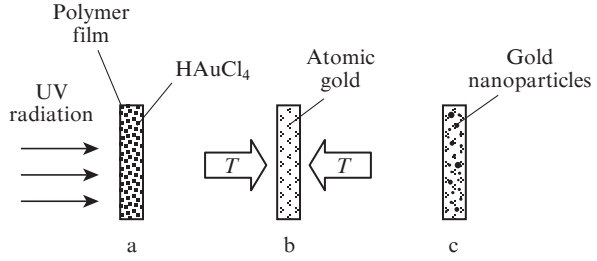

Figure 11. Schematic illustrating the preparation of gold nanoparticles in polymer film through UV exposure followed by thermostating: (a) UV irradiation of $HAuCl_4$-containing polymer film; (b) heat treatment (temperature T) of the sample containing atomic gold produced by dissociation of the acid; (c) formation of nanoparticles as a result of the heat treatment.

The nucleation and growth of gold nanoparticles were followed using attenuation coefficient measurements in the UV and visible spectral regions. Figure 12 illustrates the effect of UV irradiation on the attenuation coefficient of the composites.

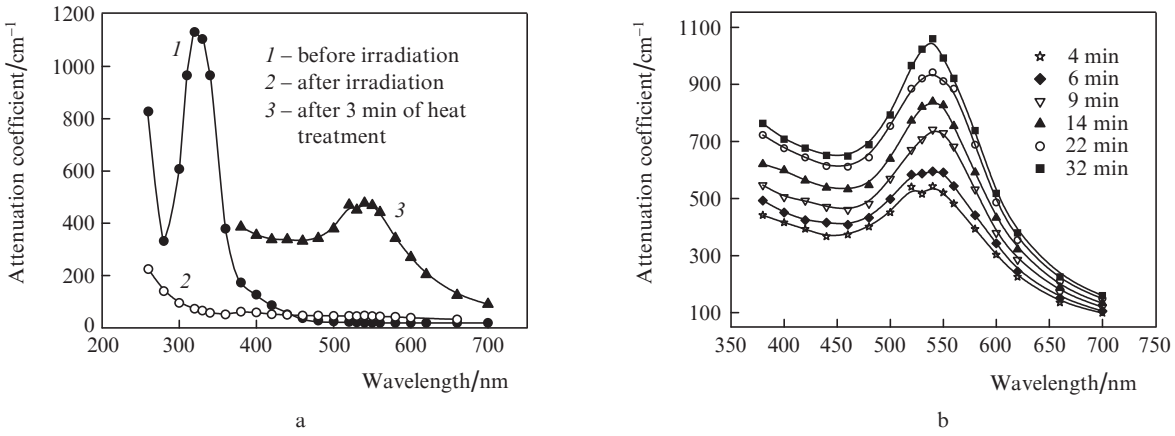

Figure 12. Effects of UV irradiation and heat treatment on the attenuation spectrum of the composite: (a) UV irradiation eliminates the peak at 320 nm, due to $HAuCl_4$, and subsequent heat treatment gives rise to a peak due to the formation of gold nanoparticles in the polymer; (b) effect of heat treatment at 75 °C on the attenuation spectrum of a 50-μm-thick PMMA film (peak-attenuation wavelength λ = 540 nm).

Also shown for comparison is the spectrum of a $HAuCl_4$-containing film before UV exposure [spectrum (*1*)].

The spectrum of the unirradiated sample has a prominent peak at 320 nm, which corresponds to the peak-absorption wavelength of $HAuCl_4$. It is clear from Fig. 12a that UV exposure leads to $HAuCl_4$ photolysis, as evidenced by the disappearance of the 320-nm peak. At the same time, there is no absorption in the visible range after this step (initiation of nanoparticle formation) [spectrum (*2*)].

Further irradiation for up to 30 min produces no significant changes in the attenuation spectrum of the film. Next, a peak emerges in the plasmon resonance region, characteristic of gold nanoparticles. According to experiments in which the composites were UV-irradiated, the only effect of UV exposure is $HAuCl_4$ photolysis, which gives a supersaturated solid solution of gold atoms in the polymer matrix. The metallic particles are formed from the supersaturated solution of gold atoms as a result of a first-order phase transition. The rate of this process is controlled by gold diffusion and, accordingly, depends significantly on temperature. In view of this, the experimental procedure was modified: the UV irradiation step, responsible for the formation of a supersaturated solid solution of gold atoms, was separated from the formation of nanoparticles during heat treatment at a certain temperature, which allowed us to examine the temperature effect on the rate of nanoparticle formation. The sample was UV-irradiated until the attenuation peak due to $HAuCl_4$ completely disappeared. Next, the irradiation was ceased and the sample was placed in a thermostat maintained at a certain temperature. The formation of nanoparticles was inferred from changes in the attenuation spectrum in the plasmon resonance region of gold nanoparticles. The time variation of the attenuation spectrum was studied in a wide temperature range (20–80 °C). Typical spectra are presented in Fig. 12b.

As seen in Fig. 12, thermostating gives rise to an attenuation peak in the plasmon resonance region of gold nanoparticles. Based on the Mie theory [59] and modern models for the size-dependent permittivity of metallic particles [60, 61], one can derive the attenuation spectrum of spherical particles, neglecting interparticle interactions. Note that the shape of the attenuation spectrum is size-dependent: with increasing particle radius, the attenuation peak grows both in magnitude and relative to the UV absorption, becomes sharper and shifts to longer wavelengths. Such changes are observed to a particle radius of 10–20 nm. At larger particle radii, the peak begins to broaden and another feature emerges, corresponding to the next mode of the plasmon resonance.

Analysis of the evolution of the attenuation spectrum during annealing demonstrates that the shape of the spectrum varies insignificantly. The same refers to the peak position and width. Since the evolution of the spectrum is associated with the formation and growth of gold nanoparticles in the film, this behaviour of the spectrum suggests that annealing increases the number density of nanoparticles, whereas the particle size distribution remains essentially unchanged.

We propose the following model for the photoinduced formation of gold nanoparticles in polymer films [62]. Absorption of a UV photon by a precursor molecule initiates a sequence of chemical reactions, leading to the reduction of gold atoms and the formation of a supersaturated solid solution of gold atoms in the polymer matrix. Subsequent decomposition of the solid solution gives gold nanoparticles, which act as nuclei of a new phase, metallic gold. Raising the annealing temperature markedly accelerates gold diffusion and, accordingly, the formation of nanoparticles. Therefore, the formation of gold nanoparticles in this model can be described in terms of the theory of first-order phase transitions.

However, attempts to describe the kinetics of gold nanoparticle formation using Zeldovich and Lifshitz–Slezov theories [63] have been unsuccessful because these theories predict a shift of the particle size distribution to larger sizes over time, i.e. an increase in average particle size, whereas in our experiments the number density of particles increased over time, but their size distribution remained unchanged. Taking into account the mechanical stress arising during nanoparticle growth does not alleviate the problem because this leads merely to renormalisation of the effective surface tension coefficient at the nanoparticle–polymer interface. Note that a heterogeneous model for nanoparticle growth upon a first-order phase transition, in which nanoparticles grow at inhomogeneities of the matrix, is also incapable of accounting for the observed steady-state distribution.

The above experimental data can be rationalised in terms of a recently proposed model [62] which takes into account the stabilising effect of the matrix. In a rate equation similar to the Fokker–Planck equation in the Zeldovich theory for

the time variation of the particle size distribution, the stabilisation effect is represented by an extra relaxation term which corresponds to a transition of a growing nanoparticle to a stabilised, inactive state with a particular transition frequency. The stabilisation leads to a steady-state particle size distribution and a monotonic increase in the total number of nanoparticles at a fixed size distribution. The attenuation spectrum calculated in the Mie theory using the shape of this distribution for particles with a radius above the critical one agrees with the measured spectrum in the optical range ($\lambda > 550$ nm). In the shorter wavelength part of the spectrum, the contribution of particles less than 5 nm in radius is significant. The size distribution function of such particles is fairly difficult to find, but this is unnecessary: it follows from the Mie theory that the absorption in gold nanoparticles in the near-UV and visible spectral regions is roughly proportional to their volume, so the net attenuation is determined by the total number of gold atoms in the nanoparticles. Taking this into account allows one to adequately describe the measured spectra (Fig. 13) and particle growth data and determine model parameters, such as the parameter related to the particle lifetime in the active state and the particle flux through the critical point in particle size space.

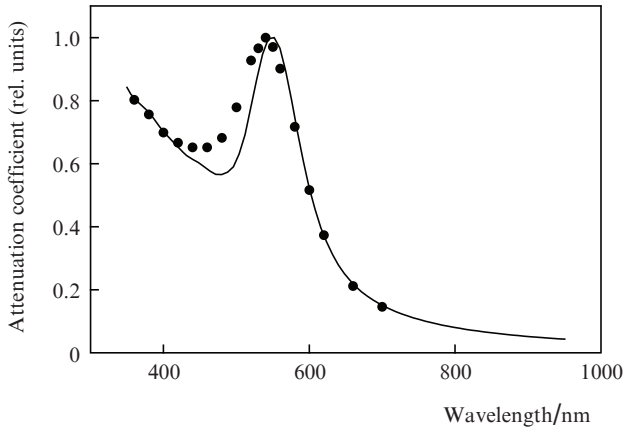

Figure 13. Comparison of the measured spectrum of an annealed film (data points) with modelling results [62] (solid curve).

As pointed out above, the synthesis of metallic nanoparticles in transparent dielectric matrices considerably changes both the linear and nonlinear optical properties of the material. That the nanocomposites described above result from photoinduced processes allows one to produce nanostructured regions of arbitrary shape and to control the properties and size distribution of the resultant clusters by adjusting the irradiation conditions. Such nanocomposites can be produced using UV lamps, but the use of laser radiation is critical for the fabrication of complex architectures within bulk materials for photonic applications.

One example of optical nanocomposite devices is so-called random lasers [64–67], in which feedback is due to scattering by nanoparticles. Popov et al. [68] reported random lasing in gold nanoparticles embedded in a polymer matrix (PMMA) containing a laser dye. But those particles were inserted into the matrix. The approach described above can in principle be used to produce random lasers in UV-irradiated regions of the material.

At the same time, the above photogeneration of gold nanoclusters in a polymer matrix presents several problems which limit the use of this technology in photonics.

One problem is the large amount of forming small particles, which make a significant contribution to the optical loss. One way to alleviate this problem is to increase the free volume in the matrix, which might cause the smallest particles to aggregate. Yakimovich et al. [69] used methyl methacrylate/2-ethylhexyl acrylate copolymers as matrices. Ethylhexyl acrylate is known to increase the free volume. Their results demonstrate that, all other factors being the same, the attenuation peak of the nanoparticles in such matrices is shifted to longer wavelengths, indicating an increase in average nanoparticle size. In general, the larger the nanoparticle, the greater is the ratio of its scattering and absorption coefficients, which is also essential for a number of applications.

Another problem is that the above procedure gives films, whereas many applications, including random laser fabrication, require bulk materials. Such materials can be produced using the polymerisation method described by Yang et al. [70]. The difficulty is that the precursors of metals have a significant effect on the polymerisation process. In particular, the most common gold precursor $HAuCl_4$ slows down the process. As a result, only a very low concentration of the precursor (5×10^{-4} M), insufficient for practical application, can be introduced into bulk materials by the method under consideration. Our group has begun to develop a technique that would enable an increase in precursor concentration (and hence in gold concentration) by at least one order of magnitude [71]. Further development of this technique will allow one to produce bulk samples of any shape and dimensions, suitable for photogeneration of gold nanoparticles.

Another example of instability resulting in 3D nanostructuring of materials is the aforementioned cavitation process during stress relief. In addition, note the laser-induced aggregation process, which also leads to nanocluster formation. This process is currently the subject of detailed studies in connection with the photoaggregation of water-soluble proteins [72, 73] as a mechanism of cataract formation.

Acknowledgements. This work was supported by the Russian Foundation for Basic Research (Grant No. 09-02-00665-a), the Presidium of the Russian Academy of Sciences (programme Ultrastrong Optical Fields and Their Applications) and the RF Ministry of Education and Science (federal targeted programme Scientists and Teachers of Innovative Russia, 2009–2013, State Contract No. 16.740.11.0018, 1 September 2010).

References

1. Novotny L., Hetch B. *Principles of Nano-Optics* (Cambridge: Cambridge University Press, 2008).
2. Lu. Y.F., Hu B., Mai Z.H., Wang W.J., Chim W.K., Chong T.C. *Jpn. J. Appl. Phys.*, **40**, 4395 (2001).
3. Chong T.C., Hong M.H., Shi L.P. *Laser Photonics Rev.*, **4**, 123 (2010).
4. Lu Y.F., Zhang L., Song W.D., Zheng Y.W., Luk'yanchuk B.S. *Pis'ma Zh. Eksp. Teor. Fiz.*, **72** (9), 658 (2000).
5. Mosbacher M., Munzer H.J., Zimmerman J., Solis J., Boneberg J., Lerderer P. *Appl. Phys. A*, **72**, 41 (2001).
6. Langer G., Brodoceanu D., Bauerle D. *Appl. Phys. Lett.*, **89**, 261104 (2006).
7. McLeod E., Arnold C.B. *Nat. Nanotechnol.*, **3**, 413 (2008).

8. Pikulin A., Bityurin N., Langer G., Brodoceanu D., Baeuerle D. *Appl. Phys. Lett.*, **91**, 191106 (2007).
9. Pikulin A., Afanasiev A., Alexandrov A., Agareva N., Korytin A., Bityurin N. *Proc. ICONO/LAT* 2010 (Kazan, 2010).
10. Wang Z.B., Guo W., Luk'yanchuk B., Whitehead D.J., Li L., Liu Z. *J. Laser Micro-Nanoengin.*, **3**, 14 (2008).
11. Karlov N.V., Kirichenko N.A., Luk'yanchuk B.S. *Lazernaya termokhimiya* (Laser Thermochemistry) (Moscow: Nauka, 1992).
12. Bityurin N. *Ann. Rep. Prog. Chem., Sect. C: Phys. Chem.*, **101**, 216 (2005).
13. Pikulin A., Bityurin N. *Phys. Rev. B*, **82**, 085406 (2010).
14. Bityurin N., Malyshev A. *J. Appl. Phys.*, **92**, 605 (2002).
15. Kamensky V., Feldchtein F., Gelikonov V., Snopova L., Muraviov S., Malyshev A., Bityurin N., Sergeev A. *J. Biomed. Opt.*, **4**, 137 (1999).
16. Malyshev A.Yu., Agareva N.A., Mal'shakova O.A., Bityurin N.M. *Opt. Zh.*, **74**, 80 (2007).
17. Malyshev A.Yu., Agareva N.A., Mal'shakova O.A., Kirsanov A., Bityurin N. *Proc. ICONO/LAT* 2007 (Minsk, 2007).
18. Fukumura H., Mibuka N., Eura S., Masuhara H. *Appl. Phys. A*, **53**, 255 (1991).
19. Beinhorn F., Ihlemann J., Luther K., Troe J. *Appl. Phys. A*, **68**, 709 (1999).
20. Phillips H.M., Sauerbrey R. *Opt. Eng.*, **32**, 2424 (1993).
21. Himmelbauer M., Arenholz E., Bäuerle D., Schilcher K. *Appl. Phys. A*, **63**, 337 (1996).
22. Himmelbauer M., Arnold N., Bityurin N., Arenholz E., Bäuerle D. *Appl. Phys. A*, **64**, 451 (1997).
23. Furutani H., Fukumura H., Masuhara H., Lippert T., Yabe A. *J. Phys. Chem. A*, **101**, 5742 (1997).
24. Masubuchi T., Furutani H., Fukumura H., Masuhara H. *J. Phys. Chem. B*, **105**, 2518 (2001).
25. Tada T., Asahi T., Tsuchimori M., Watanabe O., Masuhara H. *Jpn. J. Appl. Phys.*, **43**, 5337 (2004).
26. Krueger J., Martin S., Maedebach H., Urech L., Lippert T., Wokaun A., Kautek W. *Appl. Surf. Sci.*, **247**, 406 (2005).
27. Voisey K.T., Fouquet S., Roy D., Clyne T.W. *Opt. Lasers Eng.*, **44**, 1185 (2006).
28. Prasad M., Conforti P.F., Garrison B.J. *J. Appl. Phys.*, **101**, 103113 (2007).
29. Malyshev A., Bityurin N. *Appl. Phys. A*, **79**, 1175 (2004).
30. Malyshev A.Yu., Bityurin N.M. *Kvantovaya Elektron.*, **35**, 825 (2005) [*Quantum Electron.*, **35**, 825 (2005)].
31. Zhakhovskii V.V., Inogamov N.A., Nishihara K. *Pis'ma Zh. Eksp. Teor. Fiz.*, **87**, 491 (2008).
32. Lazare S., Bonneau R., Gaspard S., Castillejo M., Sionkowska A. *Appl. Phys. A*, **94**, 719 (2009).
33. Bityurin N. *Appl. Surf. Sci.*, **255**, 9851 (2009).
34. Takada K., Sun H.B., Kawata S. *Proc. SPIE Int. Soc. Opt. Eng.*, **6110**, 61100A (2006).
35. Park S.H., Lim T.W., Yang D.-Y., Cho N.C., Lee K.-S. *Appl. Phys. Lett.*, **89**, 173133 (2006).
36. Takada K., Sun H.-B., Kawata S. *Appl. Phys. Lett.*, **86**, 071122 (2005).
37. Farsari M., Chichkov B.N. *Nat. Photonics*, **3**, 450 (2009).
38. Strickler J.H., Webb W.W. *Opt. Lett.*, **16**, 1780 (1991).
39. Borisov R., Dorojkina G., Koroteev N., Kozenkov V., Magnitskii S., Malakhov D., Tarasishin A., Zheltikov A. *Appl. Phys. B*, **67**, 765 (1998).
40. Pikulin A., Bityurin N. *Phys. Rev. B*, **75**, 195430 (2007).
41. Bityurin N., Luk'yanchuk B.S., Hong M.H., Chong T.C. *Opt. Lett.*, **29**, 2055 (2004).
42. Englert L., Rethfeld B., Haag L., Wollenhaupt M., Sarpe-Tudoran C., Baumert T. *Opt. Express*, **15**, 17855 (2007).
43. Bityurin N., Kuznetsov A. *J. Appl. Phys.*, **93**, 1567 (2003).
44. Bityurin N., Kuznetsov A. *Proc. ICONO/LAT 2010* (Kazan, 2010).
45. Bityurin N., Znaidi L., Kanaev A. *Chem. Phys. Lett.*, **374**, 95 (2003).
46. Kuznetsov A., Kameneva O., Alexandrov A., Bityurin N., Marteau Ph., Chhor K., Sanchez C., Kanaev A. *Phys. Rev. E*, **71**, 021403 (2005).
47. Kameneva O., Kuznetsov A., Smirnova L.A., Rozes L., Sanchez C., Alexandrov A., Bityurin N., Marteau Ph., Kanaev A. *J. Mater. Chem.*, **15**, 3380 (2005).
48. Kameneva O.V., Kuznetsov A.I., Smirnova L.A., Rozes L., Sanchez K., Kanaev A., Aleksandrov A.P., Bityurin N.M. *Dokl. Akad. Nauk*, **407**, 29 (2006).
49. Kuznetsov A.I., Kameneva O., Bityurin N., Rozes L., Sanchez C., Kanaev A. *Phys. Chem. Chem. Phys.*, **11**, 1248 (2009).
50. Kuznetsov A.I., Kanaev A., Bityurin N. *Opt. Express*, **15**, 5782 (2007).
51. Daniel M.-C., Austruc D. *Chem. Rev.*, **104**, 293 (2004).
52. Buchachenko A.L. *Usp. Khim.*, **72** (5), 419 (2003).
53. Pomogailo A.D., Rozenberg A.S., Uflyand U.E. *Nanochastitsy metallov v polimerakh* (Metal Nanoparticles in Polymers) (Moscow: Khimiya, 2000).
54. Banfi G., Degiorgio V., Ricard D. *Advan. Phys.*, **47**, 447 (1998).
55. Qu S., Zhao C., Jiang X., Fang G., Gao Y., Zeng H., Song Y., Qui J., Zhu C., Hirao K. *Chem. Phys. Lett.*, **368**, 352 (2003).
56. Alexandrov A., Smirnova L., Yakimovich N., Sapogova N., Soustov L., Kirsanov A., Bityurin N. *Appl. Surf. Sci.*, **248**, 181 (2005).
57. Smirnova L.A., Aleksandrov A.P., Yakimovich N.O., Sapogova N.V., Kirsanov A.V., Soustov L.V., Bityurin N.M. *Dokl. Akad. Nauk*, **400**, 779 (2005).
58. Speranskaya T.A., Tarutina L.I. *Opticheskie svoistva polimerov* (Optical Properties of Polymers) (Leningrad: Khimiya, 1976).
59. Born M., Wolf E. *Principles of Optics* (Oxford: Pergamon, 1969; Moscow: Nauka, 1973).
60. Kreibig U., Vollmer M. *Optical Properties of Metal Clusters* (Berlin – Heidelberg – New York: Springer, 1995).
61. Johnson P.B., Christy R.W. *Phys. Rev. B*, **6**, 4370 (1972).
62. Sapogova N., Bityurin N. *Appl. Surf. Sci.*, **255**, 9613 (2009).
63. Lifshitz E.M., Pitaevskii L.P. *Physical Kinetics* (Oxford: Pergamon, 1981; Moscow: Nauka, 1979).
64. Letokhov V.S. *Zh. Eksp. Teor. Fiz.*, **5**, 262 (1967).
65. Wu X.H., Yamilov A., Noh H., Cao H., Seelig E.W., Chang R.P.H. *J. Opt. Soc. Am. B*, **21**,159 (2004).
66. Anglos D., Stassinopoulos A., Das R.N., Zacharakis G., Psyllaki M., Jakubiak R., Vaia R.A., Giannelis E.P., Anastasiadis S.H. *J. Opt. Soc. Am. B*, **21**, 208 (2004).
67. Chelnokov E.V., Bityurin N., Ozerov I., Marine W. *Appl. Phys. Lett.*, **89**, 171119 (2006).
68. Popov O., Zilbershtein A., Davidov D. *Appl. Phys. Lett.*, **89**, 191116 (2006).

69. Yakimovich N.O., Sapogova N.V., Smirnova L.A., Aleksandrov A.P., Gracheva T.A., Kirsanov A.V., Bityurin N.M. *Khim. Fiz.*, **27**, 61 (2008).

70. Yang J., Hasell T., Wang W., Howdle S.M. *Eur. Polym. J.*, **44**, 1331 (2008).

71. Agareva N.A., Aleksandrov A.P., Smirnova L.A., Bityurin N.M. *Perspekt. Mater.*, **1**, 5 (2009).

72. Soustov L.V., Chelnokov E.V., Sapogova N.V., Bityurin N.M., Nemov V.V., Sergeev Yu.V., Ostrovsky M.A. *Biofizika*, **53**, 582 (2008).

73. Chelnokov E., Soustov L., Sapogova N., Ostrovsky M., Bityurin N. *Opt. Express*, **16**, 18798 (2008).